VNU Journal of Science: Mathematics - Physics

Journal homepage: https://js.vnu.edu.vn/MaP

Original Article

Controlling Optical Properties and Optical Bistability via an External Magnetic Field in a Tripod-type Atomic Medium

Hoang Thi Huong[1], Le Nguyen Mai Anh[2], Le Thi Hoa Lai[3,4], Le Thanh Hoa[3, 5], Nguyen Van Phu[3], Thai Doan Thanh[6], Nguyen Tuan Anh[6], Hoang Minh Dong[6,*]

[1]*Bach Khoa Saigon College, 34-34A Nguyen Binh Khiem, Ho Chi Minh City, Vietnam*

[2]*Nong Lam University, Quarter 33, Linh Xuan, Ho Chi Minh City, Vietnam*

[3]*Vinh University, 182 Le Duan, Nghe An, Vietnam*

[4]*Long Huu Dong High School, 826 Provincial Road, Tay Ninh, Vietnam*

[5]*Nguyen Khuyen High School, 327 Street No. 3, Hiep Binh, Ho Chi Minh City, Vietnam*

[6]*Ho Chi Minh City University of Industry and Trade, 140 Le Trong Tan, Ho Chi Minh City, Vietnam*

Received 9th February 2026
Revised 20th April 2026; Accepted 5th May 2026

Abstract: We investigated control of optical bistability behavior based on the probe absorption and Kerr nonlinearity properties in a tripod-type degenerate four-level atom system under an external magnetic field. This excitation configuration can provide two transparent spectral regions on the probe absorption profile. It can be transitioned between the transparency and absorption regimes by turning the magnetic field on or off in different frequency domains. We can effortlessly transform one into two transparency windows, and vice versa, by adjusting the magnetic field intensity. The investigations showed the enhancement of the Kerr nonlinearity around one/two-EIT windows, thereby forming one/two-channel optical bistability in these frequency regions. In addition, the coupling field intensity, the probe frequency detuning, and the atomic cooperation parameter have also significantly influenced the absorption spectrum, Kerr nonlinearity, and optical bistability. The proposed model has useful applications in storage, optical switching, and nonlinear logic gates for optical communications processing.

Keywords: Tripod-type, light storage, transparency and absorption, Kerr nonlinearity, optical bistability.

* Corresponding author.
E-mail address: donghm@huit.edu.vn

https//doi.org/10.25073/2588-1124/vnumap.5115

1. Introduction

Light-by-light control refers to the manipulation of one optical field by another through a nonlinear medium. This functionality underpins many key photonic devices, including optical switches, optical bistability, optical logic gates, and optical memory elements, which are essential components of optical communication networks and quantum information processing systems [1-3]. Efficient light-controlled interactions remain challenging in conventional materials due to their weak and passive nonlinear responses. To overcome this limitation, various strategies have been explored, such as the development of strongly nonlinear media, the use of high-intensity control fields, and, more recently, the exploitation of electromagnetically induced transparency (EIT) media [3]. A significant advantage of EIT-based schemes is their ability to generate extremely large nonlinearities at very low light intensities, while offering flexible control via external electromagnetic or magnetic fields [4-8].

EIT originates from destructive quantum interference between different transition pathways [3]. Conversely, constructive quantum interference can enhance transition amplitudes and lead to electromagnetically induced absorption (EIA) [9]. The optical response of a medium differs markedly between these two regimes: EIT is characterized by near-complete transmission accompanied by normal dispersion, whereas EIA features strong absorption and anomalous dispersion [10-12]. Significantly, both absorption and dispersion properties can be efficiently manipulated through external control fields [13].

In addition to steep linear dispersion, EIT media exhibit strongly enhanced optical nonlinearities with suppressed absorption, enabling nonlinear optical effects at very low intensities. One prominent example is optical bistability (OB), which can be realized at low input powers owing to the giant Kerr nonlinearity associated with EIT [14-16]. Moreover, since both the magnitude and sign of the nonlinearity are tunable, the threshold and hysteresis width of OB can be effectively controlled using external fields [17-20]. With the growing interest in Kerr nonlinearity in four-level and five-level atomic systems, OB has also been studied in these configurations, where it can manifest at multiple frequencies simultaneously, such as diamond-type [17], N-type [18, 19], Y-type [20], etc. Besides that, various factors such as external magnetic fields [21, 22], polarization and relative phase of laser fields [23], and incoherent pump fields [24, 25] have been introduced to modify the threshold intensity and width of the OB effect. Nonetheless, there is still a lack of combined studies of the magnetic field and polarization between two components of the control fields on the Kerr nonlinearity and optical bistability behavior in a tripod-type degenerate atom system.

In this work, we explore light-controlled light interactions in a four-level tripod-type atomic system driven by probe, coupling, and magnetic fields. Our analytical and numerical results show the enhancement of the Kerr nonlinearity around one/two-EIT windows, thereby creating one/two-channel optical bistability in these frequency regions. We demonstrate that a threshold intensity and the width of the OB can be manipulated by altering the strength of the magnetic field, the coupling field intensity, and the probe frequency detuning. These results provide clear physical insight into the interplay between linear and nonlinear optical processes in multi-level atomic systems, which have applications for optical switching, storage, and nonlinear logic gates in optical communications.

2. Model and Basic Equations

Figure 1 illustrates an energy-degenerate tripod configuration four-level system interacting with a pair of laser fields [13, 17]. The probe beam E_p exhibits linear polarization and low intensity, oscillating at frequency ω_p with coupling strength quantified by the Rabi frequency $2\Omega_p = \mu_{41}E_p/\hbar$, and it

addresses the $|4\rangle \leftrightarrow |1\rangle$ transition. In parallel, an intense elliptically polarized coupling field (EPF) E_c, carrier frequency ω_c, possessing Rabi frequencies $2\Omega_c = \mu_{4j}E_c/\hbar$ (where j = 2, 3), links state $|4\rangle$ with states $|2\rangle$ and $|3\rangle$ through its left- and right-circularly polarized components, which respectively drive the $|4\rangle \leftrightarrow |2\rangle$ and $|4\rangle \leftrightarrow |3\rangle$ transitions. The overall structure effectively reduces to two coupled Λ configurations linked by the common probe field E_p. One Λ-subsystem involves the state triplet $|4\rangle$, $|2\rangle$, $|1\rangle$, while the other encompasses $|4\rangle$, $|3\rangle$, $|1\rangle$. Application of a magnetic field B along the laser beam axis produces Zeeman-induced energy splitting within the excited state manifold. We begin with atoms in the ground state $|1\rangle$ where $\rho_{11} = 1$ [30]. The excited state manifold experiences Zeeman-induced energy splitting, quantified by $\hbar\Delta_B = \mu_B m_F g_F B$. Here, μ_B and g_F are the Bohr magneton and Landé factors, respectively, with $m_F = \pm 1$ serving as the magnetic quantum number for each sub-level. Within the interaction picture and applying rotating-wave plus electric dipole approximations, the system Hamiltonian (setting $\hbar$=1) takes the form:

$$\hat{H} = \Delta_p|4\rangle\langle 4| + \left(\Delta_p - \Delta_c + \Delta_B\right)|3\rangle\langle 3| + \left(\Delta_p - \Delta_c - \Delta_B\right)|2\rangle\langle 2| + \left[\Omega_p|4\rangle\langle 1| + \Omega_{c^-}|4\rangle\langle 2| + \Omega_{c^+}|4\rangle\langle 3| + H.c\right] \quad (1)$$

The notation *H.c.* signifies Hermitian conjugate operation, and the notations: $\Delta_p = \omega_{41} - \omega_p$, and $\Delta_c = \omega_{42} - \omega_c - \Delta_B = \omega_{43} - \omega_c + \Delta_B$, are the detunings of the probe and control fields from the corresponding two-level transitions; the Zeeman energy separation between $|2\rangle$ and $|3\rangle$ states equal $2\Delta_B$ [refer to Fig. 1].

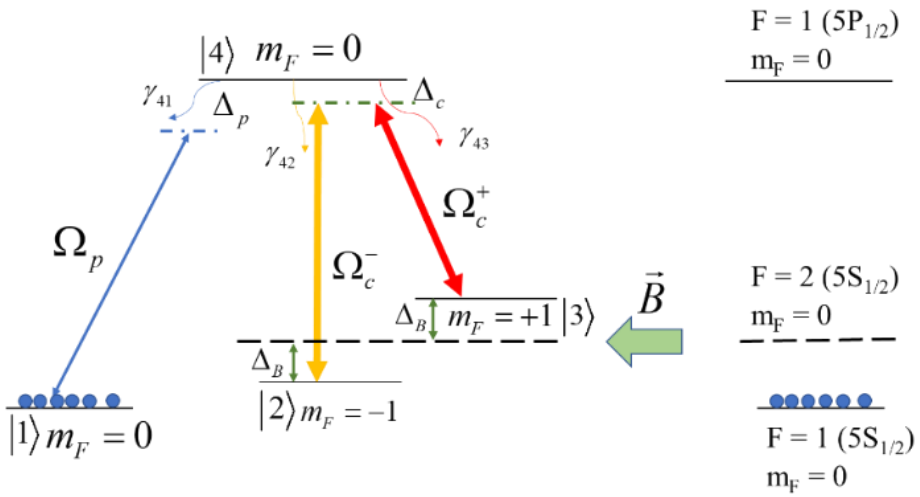

Figure 1. The illustrated four-level tripod atomic system operates within a static magnetic field medium, displaying the corresponding energy level configuration.

Temporal dynamics of the system are governed by the Liouville equation [17].

$$\frac{\partial\rho}{\partial t} = -i\left[H_{\text{int}}, \rho\right] + \Lambda\rho \quad (2)$$

By combining Hamiltonian (1) with Liouville equation (2), we derive the following density matrix equation set:

$$\dot{\rho}_{11} = \gamma_1\rho_{44} - i\Omega_p\rho_{14} + i\Omega_p^*\rho_{41}, \quad (3a)$$

$$\dot{\rho}_{22} = \gamma_2\rho_{44} - i\Omega_c^{-}\rho_{24} + i\Omega_c^{-*}\rho_{42}, \tag{3b}$$

$$\dot{\rho}_{33} = \gamma_3\rho_{44} - i\Omega_c^{+}\rho_{34} + i\Omega_c^{+*}\rho_{43}, \tag{3c}$$

$$\dot{\rho}_{44} = -(\gamma_1+\gamma_2+\gamma_3)\rho_{44} + i\Omega_p\rho_{14} - i\Omega_p^{*}\rho_{41} + i\Omega_c^{-}\rho_{24} - i\Omega_c^{-*}\rho_{42} + i\Omega_c^{+}\rho_{34} - i\Omega_c^{+*}\rho_{43}, \tag{3d}$$

$$\dot{\rho}_{41} = -\left(\gamma_{41} + i\Delta_p\right)\rho_{41} - i\Omega_p(\rho_{44}-\rho_{11}) + i\Omega_c^{-}\rho_{21} + i\Omega_c^{+}\rho_{31}, \tag{3e}$$

$$\dot{\rho}_{42} = -\left(\gamma_{42} + i\left(\Delta_c+\Delta_B\right)\right)\rho_{42} + i\Omega_p\rho_{12} + i\Omega_c^{+}\rho_{32} - i\Omega_c^{-}(\rho_{44}-\rho_{22}), \tag{3f}$$

$$\dot{\rho}_{43} = -\left(\gamma_{43} + i\left(\Delta_c-\Delta_B\right)\right)\rho_{41} + i\Omega_p\rho_{13} + i\Omega_c^{-}\rho_{23} - i\Omega_c^{+}(\rho_{44}-\rho_{33}), \tag{3g}$$

$$\dot{\rho}_{21} = -\left(\gamma_{21} + i\left(\Delta_p-\Delta_c-\Delta_B\right)\right)\rho_{21} - i\Omega_p\rho_{24} + i\Omega_c^{-*}\rho_{41}, \tag{3h}$$

$$\dot{\rho}_{31} = -\left(\gamma_{31} + i\left(\Delta_p-\Delta_c+\Delta_B\right)\right)\rho_{31} - i\Omega_p\rho_{34} + i\Omega_c^{+*}\rho_{41}, \tag{3i}$$

$$\dot{\rho}_{32} = -\left(\gamma_{32} + 2i\Delta_B\right)\rho_{32} - i\Omega_c^{-}\rho_{34} + i\Omega_c^{+*}\rho_{42}, \tag{3j}$$

where $\rho_{11}+\rho_{22}+\rho_{33}+\rho_{44}=1$ and $\rho_{ij}=\rho_{ji}^{*}(i\neq j)$. The population and dephasing decay rates are phenomenologically added to the above density-matrix equations [13]. The population decay rates from the excited state $|4\rangle$ to the ground states $|1\rangle$, $|2\rangle$, and $|3\rangle$ are γ_1, γ_2, and γ_3, respectively. The decay rate between the states $|4\rangle$ and $|j\rangle$ is γ_{4j} (j = 1, 2, 3), and we have the relationship $\gamma_{4j}=\left(\gamma_{41}+\gamma_{42}+\gamma_{43}\right)/2$: the dephasing decay rates between the ground-state coherences are γ_{31}, γ_{32} and γ_{21}.

To obtain the steady-state solutions for the density matrix element ρ_{41}) in higher-order perturbations, we need to use a iterative technique in which the density matrix elements are expressed as [8] , where each successive approximation is calculated using the matrix elements of one order lower than the one being calculated. Applying the above iterative technique to the third-order perturbation, the solution of the density matrix element ρ_{41} in the third-order perturbation as:

$$\rho_{41} = \rho_{41}^{(1)} + \rho_{41}^{(3)} = \frac{i\Omega_p}{F} - \frac{2i\Omega_p^3}{\gamma_{41}F}\left(\frac{1}{F}+\frac{1}{F^*}\right), \tag{4}$$

with

$$F = \gamma_{41} + i\Delta_p + \frac{\left|\Omega_c^{-}\right|^2}{\gamma_{21}+i\left(\Delta_p-\Delta_c-\Delta_B\right)} + \frac{\left|\Omega_c^{+}\right|^2}{\gamma_{31}+i\left(\Delta_p-\Delta_c+\Delta_B\right)} \tag{5}$$

where, F^* is the complex conjugate of F. In this case, the expression for first- and third-order electric susceptibility takes the form, respectively:

$$\chi^{(1)} = \frac{N\left|\mu_{21}\right|^2}{\varepsilon_0\hbar\Omega_p}\rho_{41}^{(1)} = \frac{iN\left|\mu_{41}\right|^2}{\varepsilon_0\hbar}\frac{1}{F} \tag{6}$$

$$\chi^{(3)} = \frac{N\left|\mu_{41}\right|^2}{3\varepsilon_0\hbar\Omega_p^3}\rho_{41}^{(3)} = -\frac{iN\left|\mu_{41}\right|^4}{6\varepsilon_0\hbar^3\gamma_{41}}\frac{1}{F}\left(\frac{1}{F}+\frac{1}{F^*}\right) \tag{7}$$

where N is the atomic density and ε_0 is the permittivity in vacuum.

We know that the Kerr nonlinear refractive index n_2 is proportional to the third-order susceptibility to the probe field [11]:

$$n_2 = \frac{3\,\mathrm{Re}\left(\chi^{(3)}\right)}{4\varepsilon_0 n_0^2 c}. \tag{8}$$

with $$n_0 = \sqrt{1+\mathrm{Re}\left(\chi^{(1)}\right)}, \tag{9}$$

Now, consider a sample containing N atoms positioned within a unidirectional ring cavity, as depicted in Fig. 2. Mirrors M_3 and M_4 are assumed to be perfectly reflective, whereas mirrors M_1 and M_2 have reflection and transmission coefficients R and T, with $T + R = 1$, respectively. Only the probe field E_p is transmitted through the cavity, while the coupling field E_c is not. When that total electromagnetic field can be written:

$$E = E_p e^{-i\omega_p t} + E_c e^{-i\omega_c t} + c.c.,. \tag{10}$$

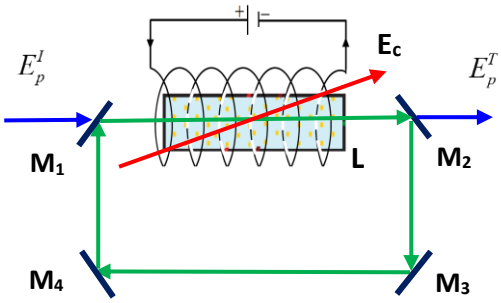

Figure 2. The single-direction ring cavities have an atomic sample length of L and contain N atoms. The E_p^I represents the incident field and E_p^T represents the transmission field.

By applying a slowly varying envelope approximation, the propagation dynamics of the probe field are derived from the Maxwell equations:

$$\frac{\partial E_p}{\partial t} + c\frac{\partial E_p}{\partial z} = i\frac{\omega_p}{2\varepsilon_0} P\left(\omega_p\right). \tag{11}$$

where $P\left(\omega_p\right)$ is induced polarization in the transition $|1\rangle \leftrightarrow |2\rangle$:

$$P\left(\omega_p\right) = N\mu_{41}\rho_{41}. \tag{12}$$

At the steady-state limit, considering the parameters of a perfectly tuned cavity, the interface conditions between the incident field E_p^I and the transmitted field E_p^I can be described as follows [21]:

$$E_p(L) = E_p^T/\sqrt{T}, \quad E_p(0) = \sqrt{T}E_p^I + RE_p(L), \tag{13}$$

The bistability behavior is caused by the reflection mechanism of mirror M_2, so that if $R = 0$, there is no bistability. Using equation (13), which combines the mean-field limit and boundary conditions, we can obtain the input-output relationship.

$$y = x - iC\rho_{41}, \tag{14}$$

where $y = \mu_{41}E_p^I / \hbar\sqrt{T}$ and $x = \mu_{41}E_p^T / \hbar\sqrt{T}$ are the normalization of the fields, and $C = \frac{\omega_p NL|\mu_{41}|^2}{2\varepsilon_0 \hbar cT}$ is the cooperation parameter. Therefore, probe absorption, Kerr nonlinearity and OB behaviors can be defined by system parameters through Eqs. (3), (6), (7) and (14).

3. Results and Discussion

The above model can be applied to ^{87}Rb atoms. We are considering the transitions between the states $5S_{1/2}$–$5P_{1/2}$, where levels $|1\rangle$, $|2\rangle$, $|3\rangle$ and $|4\rangle$ correspond to energy states ($|1\rangle = |5S_{1/2}, F = 1, m_F = 0\rangle$, $|2\rangle = |5S_{1/2}, F = 2, m_F = +1\rangle$, $|3\rangle = |5S_{1/2}, F = 2, m_F = -1\rangle$, $|4\rangle = |5P_{1/2}, F = 2, m_F = 0\rangle$), with $\gamma_1 = \gamma_2 = \gamma_3 = 2\pi \times 5.3$ MHz, $\gamma_{21} = \gamma_{31} = \gamma_{32} = 2\pi \times 0.05$ MHz, $\mu_{41} = 2.5$ x10^{-29} C.m, $g_F = -1/2$, $N = 5\times10^{17}$ atoms/m^3, and $\mu_B = 9.27401\times10^{-24}$ JT^{-1} [8, 13, 26]. For convenience in simulation calculation, we normalize all parameters with $\gamma_3 = \gamma_2 = \gamma_1 = \gamma$. Accordingly, when the Zeeman shift Δ_B is scaled by γ, the magnetic field intensity (B) is calculated by $\gamma_c = \hbar\mu_B^{-1}g_F^{-1}\gamma$. These parameters selected will be used for the analysis and simulation of probe absorption, Kerr nonlinearity and OB behaviors below.

3.1. Controlling Absorptive and Kerr Nonlinear Properties

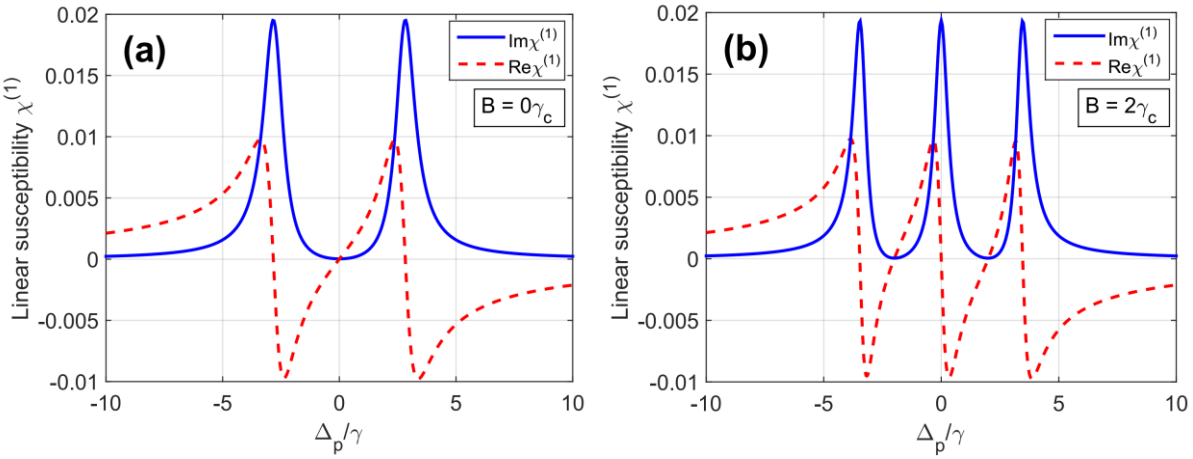

Figure 3. Graph of the probe field linear susceptibility versus probe frequency detuning Δ_p at different magnetic field intensities: B = 0 (solid line) and B = 2γ_c (dashed line). Other parameters are: $\Omega_c^- = \Omega_c^+ = 2\gamma$, $\Omega_p = 0.01\gamma$, $\Delta_c = 0$, respectively.

We first investigated the influence of the magnetic field on the first-order absorption and dispersion spectra of the probe field through the real and imaginary parts of the linear susceptibilities (, as depicted in Fig. 3. The parameters were fixed at $\Omega_p = 0.01\gamma$, $\Omega_c^- = \Omega_c^+ = 2\gamma$, $\Delta_c = 0$. Specifically, in the absence of a magnetic field B = 0, the probe response remains transparent at resonance (see the blue solid curve in Fig. 3(a)). When the magnetic field is applied, B = 2γ_c, the EIT window splits into two regions symmetric about the resonance frequency (see the blue solid curve in Fig. 3(b)), and at exact resonance, transparency is converted into absorption. Thus, by switching the magnetic field on and off, the probe response can be toggled between transparent and absorptive regimes. This effect also leads to a transition between normal dispersion, corresponding to the transparent region, and anomalous dispersion,

corresponding to the absorptive region, as depicted by the red dashed curve in Fig. 3(a, b). In particular, the normal dispersion at resonance in the absence of the magnetic field is converted into anomalous dispersion when the magnetic field is present. In contrast, the sidebands, which exhibit anomalous dispersion without the magnetic field, switch to normal dispersion when the magnetic field is applied. Furthermore, both the amplitude and slope of the normal dispersion curves in the transparency regions can be tuned by varying the magnetic field intensity.

Figure 4 illustrates the variation of the real and imaginary parts of the nonlinear susceptibilities χ, the parameters selected are similar to those in Fig. 3. As shown by the red dashed curve in Fig. 4, in the absence of the magnetic field (B = 0), a pair of enhanced Kerr nonlinear peaks appears around the resonance frequency. When the magnetic field is applied (B = $2\gamma_c$), two pairs of nonlinear peaks emerge corresponding to the two transparency regions around resonance. Thus, the presence of the magnetic field leads to the emergence of multiple enhanced Kerr nonlinear peaks at different frequency regions, thereby broadening the overall domain of enhanced Kerr nonlinearity. Such controllability may enable tunable applications of this Kerr nonlinear medium, for instance, in optical bistability systems, which will be discussed below.

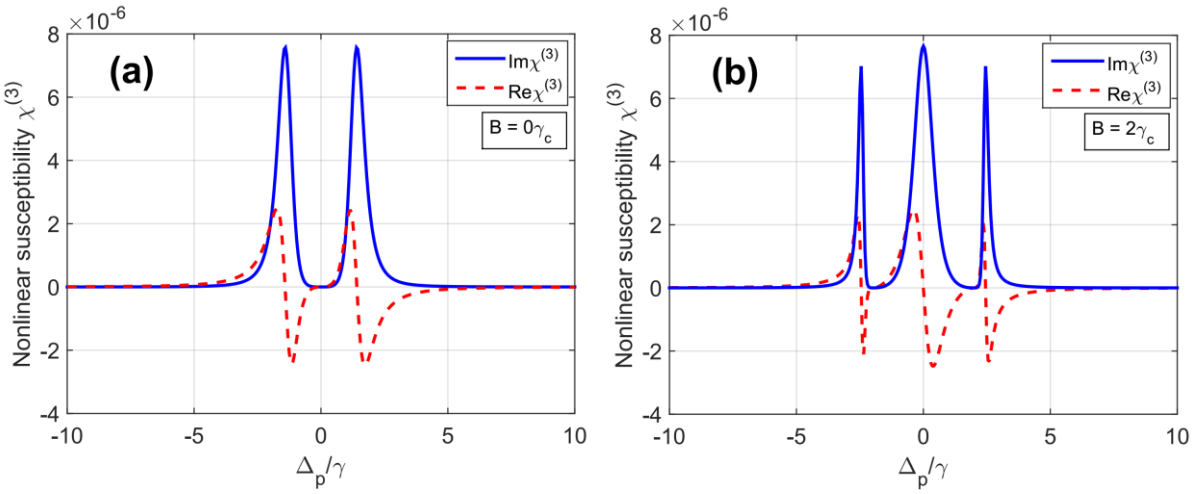

Figure 4. Graph of the probe field nonlinear susceptibility versus probe frequency detuning Δ_p at different magnetic field intensities: B = 0 (solid line) and B = $2\gamma_c$ (dashed line). Other parameters are: $\Omega_c^- = \Omega_c^+ = 2\gamma$, $\Omega_p = 0.01\gamma$, $\Delta_c = 0$, respectively.

3.2. Controlling Optical Bistability Behaviors Via Magnetic Field and System Parameters

In Fig. 5, we demonstrate that both the threshold intensity and the width of probe optical bistability (OB) can be controlled by the magnetic field (a) and frequency detuning (b) of the probe field, with the control-field intensity and detuning fixed at $\Omega_c^- = \Omega_c^+ = 2\gamma$, $\Delta_c = 0$. The variation of OB behavior with different external magnetic field B is shown in Fig. 5(a). These graphs illustrate the variation in input-output relationship curves under different external magnetic field intensities B. The width and threshold for triggering OB increase the rise of the magnetic field intensity at position $\Delta_p = 0$, demonstrating a strong interplay between the magnetic field and optical properties. In contrast, when the magnetic field is fixed at B = $2\gamma_c$, increasing the probe detuning leads to a reduction in both the threshold and the bistability width, and the OB nearly disappears when $\Delta_p = \pm 2\gamma$, as depicted in Fig. 5(b). The underlying physical mechanism can be understood by examining the absorption and Kerr nonlinear dispersion

behaviors discussed in Figs. 3 and 4. At $\Delta_p = 0$, enhanced absorption and nonlinear dispersion arise with increasing magnetic field due to the formation of a double dark resonance. Conversely, at $\Delta_p = \pm 2\gamma$, both quantities decrease as the magnetic field grows, which is attributed to the shift to the center of the two side EIT windows. These results highlight the crucial role of the external magnetic field in regulating absorption and Kerr nonlinearity, thereby providing an efficient means to control optical bistability in the system.

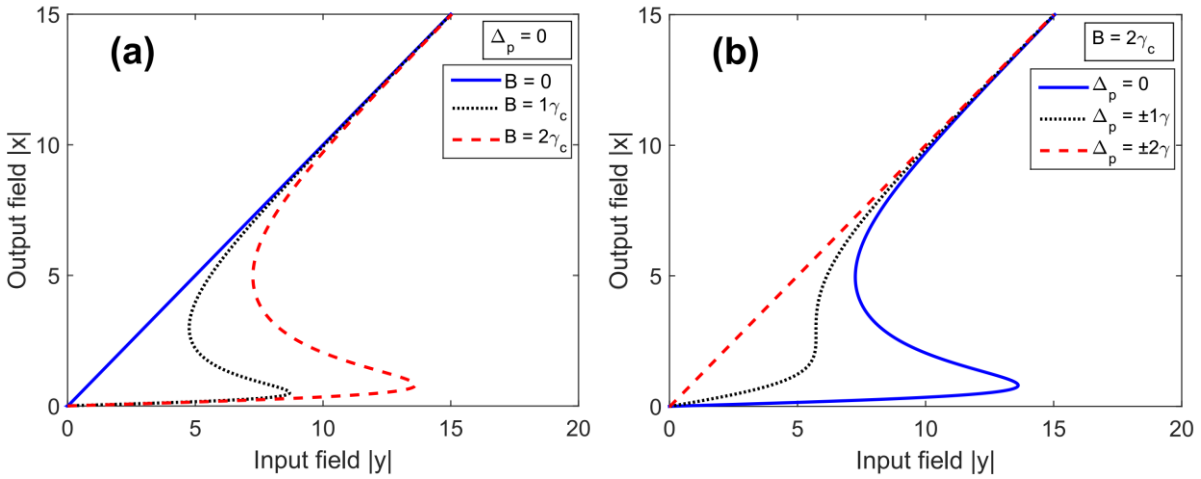

Figure 5. Graphs of the optical bistability at different values of magnetic field B when $\Delta_p = 0$ (a), and at different values of probe laser detuning Δ_p when $B = 2\gamma_c$ (b). The parameters chosen are: $\Omega_c^- = \Omega_c^+ = 2\gamma$, $\Delta_c = 0$, and C = 100, respectively.

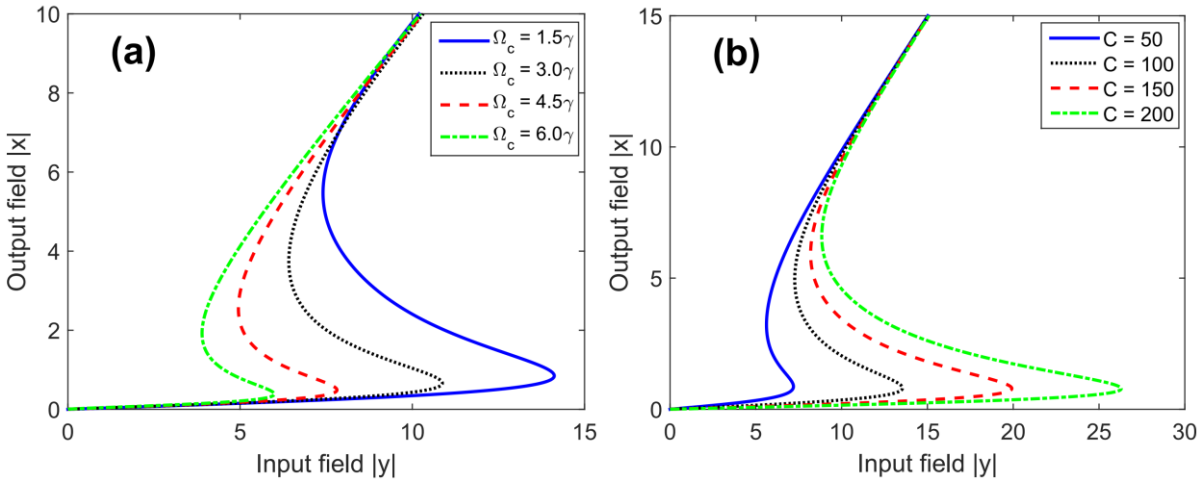

Figure 6. Graphs of the optical bistability for different values of coupling field intensity $\Omega_c^- = \Omega_c^+ = \Omega_c$ when C = 100 (a), and cooperation parameters C when $\Omega_c^- = \Omega_c^+ = 2\gamma$ (b). The parameters chosen are $B = 2\gamma_c$, and $\Delta_p = \Delta_c = 0$, respectively.

Finally, the influence of other parameters on OB can also be analyzed, as depicted in Fig. 6. In Fig. 6(a) displays the variation curves of the input-output relationship under different coupling field

intensities $\Omega_c^- = \Omega_c^+ = \Omega_c$. It can be observed that when the coupling field intensity increases, the threshold of the OB curves decreases, but the OB phenomenon continues to persist. The essence of this behavior can be understood as follows: when Ωc increases, the double dark resonance phenomenon decreases, but it still exists; the absorption at the atomic resonance center also decreases. Thus, the OB threshold is reduced without disappearing. Fig. 6(b) shows the variation curves of the input-output relationship under different cooperation parameters C. It can be seen that the magnitude of the cooperation parameter significantly affects the OB phenomenon. As the cooperation parameter increases, the OB phenomenon stays, but the threshold of the OB curve becomes larger.

Before ending this work, we outline a potential experimental realization of our proposed scheme, which is applied to the ^{87}Rb atoms on the $5S_{1/2}$-$5P_{1/2}$, transitions (see Fig. 1). The chosen states are: ($|1\rangle = |5S_{1/2}, F = 1, m_F = 0\rangle$, $|2\rangle = |5S_{1/2}, F = 2, m_F = +1\rangle$, $|3\rangle = |5S_{1/2}, F = 2, m_F = -1\rangle$, $|4\rangle = |5P_{1/2}, F = 2, m_F = 0\rangle$), with $\gamma_1 = \gamma_2 = \gamma_3 = 2\pi \times 5.3$ MHz, $\gamma_{21} = \gamma_{31} = \gamma_{32} = 2\pi \times 0.05$ MHz, $\mu_{41} = 2.5 \times 10^{-29}$ C.m, $g_F = -1/2$, $N = 5\times10^{17}$ atoms/m^3, and $\mu_B = 9.27401\times10^{-24}$ JT^{-1} [5, 17, 26]. Before interacting with atoms, the linearly polarized probe laser (795 nm) coupling the $|4\rangle\leftrightarrow|1\rangle$ transition, and the circularly polarized control laser (795nm) driving the $|4\rangle\leftrightarrow|2\rangle$, $|3\rangle$ transitions, which can be obtained from external cavity diode lasers, pass through an acousto-optic modulator (AOM) and can be operated individually. To obtain the two polarized components of the control field Ω_c^- and Ω_c^+, one can let the control beam pass through a half-wave plate (HWP) and a quarter-wave plate (QWP), in turn properly. Thus, the QWP can modulate the strengths of the coupling-field-polarized components (Ω_c^- and Ω_c^+) [5, 17].

4. Conclusion

This study has controlled the probe absorption spectrally and Kerr nonlinearity in a degenerate tripod-type four-level atomic medium by utilizing an external magnetic field and applied fields. We conducted one/two-EIT window profiles by modifying the intensity of the magnetic field or coupling laser frequencies in different frequency domains. Results have shown that enhancing the Kerr nonlinearity around one/two-EIT windows creates the one/two-channel optical bistability in these frequency regions. In addition, the coupling field intensity, the probe frequency detuning, and the atomic cooperation parameter have also significantly influenced the absorption spectrum, Kerr nonlinearity, and optical bistability. The proposed approach has useful applications for storage and optical switching, and nonlinear logic gates in optical communications.

Acknowledgments

This work was supported by the Vietnam National Foundation for Science and Technology Development (NAFOSTED) under Grant No. 103.03-2025.99.

References

[1] B. Li, S. J. Chua, Optical Switches: Materials and Design, Woodhead Publishing Limited, Cambridge, 2010.
[2] D. R. Solli, B. Jalali, Analog Optical Computing, Nat. Photonics, Vol. 9, No. 11, 2015, pp. 704-706, https://doi.org/10.1038/s41586-025-09430-z.
[3] M. Fleischhauer, A. Imamoglu, J. P. Marangos, Electromagnetically Induced Transparency: Optics in Coherent Media, Rev. Mod. Phys., Vol. 77, 2005, pp. 633-673, https://doi.org/10.1103/RevModPhys.77.633.

[4] A. M. C. Dawes, L. Illing, S. M. Clark, et al., All-Optical Switching in Rubidium Vapor, Science, Vol. 308, 2005, pp. 672-674, https://doi.org/10.1126/science.11101.
[5] S. H. Asadpour, A. E. Majd, Controlling the Optical Bistability and Transmission Coefficient in a Four-Level Atomic Medium, J. Lumin., Vol. 132, 2012, pp. 1477-1482, https://doi.org/10.1016/j.jlumin.2012.01.018.
[6] A. H. M. Abdelaziz, A. K. Sarma, Effective Control and Switching of Optical Multistability in a Three-Level V-Type Atomic System, Phys. Rev. A, Vol. 102, 2020, pp. 043719, https://doi.org/10.1103/PhysRevA.102.043719.
[7] Y. Duan, G. Lin, S. Zhang, Y. Niu, S. Gong, Low Light Level All-Optical Switching in a Four-Level Atom-Cavity System, Opt. Commun., Vol. 358, 2016, pp. 73-76, https://doi.org/10.1016/j.optcom.2015.09.043.
[8] H. M. Dong, Knob of Swapping Between Slow and Fast Light in an Inhomogeneously Broadened Medium by a Static Magnetic Field, Phys. Letts. A, Vol. 519, 2024, pp. 129715, https://doi.org/10.1016/j.physleta.2024.129715.
[9] K. Yadav, A. Wasan, Switching from EIT to EIA in a Four-Level N-Type Atomic System, Journal of Optics, Vol. 48, 2019, pp. 65, https://doi.org/10.1007/s12596-018-0495-5.
[10] H. R. Hamedi, G. Juzeliunas, Phase-Sensitive Kerr Nonlinearity for Closed-Loop Quantum Systems, Phys. Rev. A, Vol. 91, 2015, pp. 053823, https://doi.org/10.1103/PhysRevA.91.053823.
[11] H. M. Dong, N. T. Anh, T. D. Thanh, Controllable Kerr Nonlinearity in a Degenerate V-Type Inhomogeneously Broadening Atomic Medium Aided by a Magnetic Field, Opt. Quant. Electron., Vol. 54, No. 4, 2022, pp. 225, https://doi.org/10.1007/s11082-022-03593-z.
[12] H. Liang, Y. P. Niu, L. Deng, S. Q. Gong, Enhancement of Kerr Nonlinearity Completely Without Absorption, Phys. Lett. A, Vol. 381, 2017, pp. 3978-3982, https://doi.org/10.1016/j.physleta.2017.10.048.
[13] H. M. Dong, T. D. Thanh, N. T. T. Hien, L. T. Y. Nga, N. H. Bang, Controlling Optical Switching by an External Magnetic Field in a Degenerate Vee-Type Atomic Medium, Physics Letters A, Vol. 469, 2023, pp. 128765, https://doi.org/10.1016/j.physleta.2023.1287.
[14] H. R. Hamedi, A. H. Gharamaleki, M. Sahrai, Colossal Kerr Nonlinearity Based on Electromagnetically Induced Transparency in a Five-Level Double-Ladder Atomic System, Appl. Opt., Vol. 55, No. 22, 2016, pp. 5892, https://doi.org/10.1364/AO.55.005892.
[15] J. Sheng, X. Yang, H. Wu, M. Xiao, Modified Self-Kerr-Nonlinearity in a Four-Level N-Type Atomic System, Phys. Rev. A, Vol. 84, 2011, pp. 053820, https://doi.org/10.1103/PhysRevA.84.053820.
[16] J. Kou, R. G. Wan, Z. H. Kang, H. H. Wang, L. Jiang, X. J. Zhang, Y. Jiang, J. Y. Gao, EIT-Assisted Large Cross-Kerr Nonlinearity in a Four-Level Inverted-Y Atomic System, J. Opt. Soc. Am. B, Vol. 27, No. 10, 2010, pp. 2035, https://doi.org/10.1364/JOSAB.27.002035.
[17] D. Zhang, R. Yu, J. Li, C. Ding, X. Yang, Laser-Polarization-Dependent and Magnetically Controlled Optical Bistability in Diamond Nitrogen-Vacancy Centers, Phys. Lett. A, Vol. 377, 2013, pp. 2621, https://doi.org/10.1016/j.physleta.2013.07.039.
[18] M. A. Anton, F. Carreno, O. G. Calderon, S. Melle, I. Gonzalo, Optical Switching by Controlling the Double-Dark Resonances in a N-Tripod Five-Level Atom, Opt. Commun., Vol. 281, 2008, pp. 6040, https://doi.org/10.1016/j.optcom.2008.09.049.
[19] J. H. Li, X. Y. Lu, J. M. Luo, Q. J. Huang, Optical Bistability and Multistability via Atomic Coherence in an N-Type Atomic Medium, Phys. Rev. A, Vol. 74, 2006, pp. 035801, https://doi.org/10.1103/PhysRevA.74.035801.
[20] M. Sahrai, H. R. Hamedi, M. Memarzadeh, Kerr Nonlinearity and Optical Multistability in a Four-Level Y-Type Atomic System, J. Mod. Opt., Vol. 59, No. 11, 2012, pp. 980-987, https://doi.org/10.1080/09500340.2012.684443.
[21] H. M. Dong, N. H. Bang, L. V. Doai, L. T. Y. Nga, Knob of Adjusting Switching and Optical Multistability by Static Magnetic Field Under the Relative Phase in a V-Type Degenerate Medium, Chaos Solit. Fractals, Vol. 199, 2025, pp. 116914, https://doi.org/10.1016/j.chaos.2024.116914.
[22] Y. Mu, L. Qin, Z. Shi, G. Huang, Giant Kerr Nonlinearities and Magneto-Optical Rotations in a Rydberg-Atom Gas Via Double Electromagnetically Induced Transparency, Phys. Rev. A, Vol. 103, 2021, pp. 043709, https://doi.org/10.1103/PhysRevA.103.043709.
[23] S. H. Asadpour, H. R. Soleimani, Polarization Dependence of Optical Bistability in the Presence of External Magnetic Field, Opt. Commun., Vol. 310, 2014, pp. 120-124, https://doi.org/10.1016/j.optcom.2013.07.051.
[24] H. F. Xu, Optical Bistability and Multistability via both Coherent and Incoherent Fields in a Three-Level System, Laser Phys., Vol. 29, 2019, pp. 015205, https://doi.org/10.1088/1555-6611/aaed92.
[25] H. Jafarzadeh, M. Sahrai, K. Ghaleh, Controlling the Optical Bistability in a Λ-Type Atomic System via Incoherent Pump Field, Appl. Phys. B, Vol. 117, 2014, pp. 927-933, https://doi.org/10.1007/s00340-014-5910-z.
[26] D. Steck, ^{87}Rb D line data, http://steck.us/alkalidata (accessed on: January 21st, 2026).